Statistics in Medicine

WILEY

Statistics in Medicine

RESEARCH ARTICLE

Mediation Analysis with Multiple Exposures and Multiple Mediators

Yi Zhao

Department of Biostatistics and Health Data Science, Indiana University School of Medicine, Indianapolis, Indiana, USA

Correspondence: Yi Zhao (yz125@iu.edu)

Received: 10 January 2023 | **Revised:** 25 April 2024 | **Accepted:** 23 August 2024

Funding: This work was supported by National Institute of Mental Health (R01MH126970); National Institute on Aging (P30AG072976, U54AG065181).

Keywords: linear structural equation modeling | mediation analysis | multiview data integration | projection method

ABSTRACT

A mediation analysis approach is proposed for multiple exposures, multiple mediators, and a continuous scalar outcome under the linear structural equation modeling framework. It assumes that there exist orthogonal components that demonstrate parallel mediation mechanisms on the outcome, and thus is named principal component mediation analysis (PCMA). Likelihood-based estimators are introduced for simultaneous estimation of the component projections and effect parameters. The asymptotic distribution of the estimators is derived for low-dimensional data. A bootstrap procedure is introduced for inference. Simulation studies illustrate the superior performance of the proposed approach. Applied to a proteomics-imaging dataset from the Alzheimer's disease neuroimaging initiative (ADNI), the proposed framework identifies protein deposition – brain atrophy – memory deficit mechanisms consistent with existing knowledge and suggests potential AD pathology by integrating data collected from different modalities.

1 | INTRODUCTION

In this study, a mediation analysis framework for cases with multiple exposures, multiple mediators, and a continuous scalar outcome is introduced. It assumes that there exist orthogonal components that constitute parallel mediation mechanisms on the outcome, and thus is named principal component mediation analysis (PCMA), where "parallel" means that the mediation paths (or mechanisms) are independent of each other (as presented in Figure 1). Linear structural equation models are proposed for such parallel mechanisms and likelihood-based estimators are proposed for simultaneous identification of the component projections and estimation of the model coefficients.

The proposed framework is motivated by a proteomic-imaging study from the Alzheimer's disease neuroimaging initiative (ADNI). AD is an irreversible neurodegenerative disease. In 2021, an estimate of 6.5 million American aged 65 and older are living with AD and this number is projected to grow to 15.0 million by 2060 [1]. As there exists no effective treatment for AD, understanding the disease pathology, identifying treatment targets, and developing early diagnosis and intervention strategies are critically important. The ADNI was launched in 2003 aiming to identify AD biomarkers and measure the disease progression through multiple modalities, including magnetic resonance imaging (MRI), positron emission tomography (PET), other biological specimens, and clinical and neuropsychological assessments. In this study, we focus on two modalities, the cerebrospinal fluid (CSF) proteomics, and T1-weighted MR brain images, and investigate the connections between modalities, as well as to neural cognitive behaviors. It is widely known that amyloid-β (Aβ) and tau are two key protein markers for AD,

The Alzheimer's Disease Neuroimaging Initiative: Data used in preparation of this article were obtained from the Alzheimer's Disease Neuroimaging Initiative (ADNI) database (https://adni.loni.usc.edu). As such, the investigators within the ADNI contributed to the design and implementation of ADNI and/or provided data but did not participate in analysis or writing of this report. A complete list of ADNI investigators can be found at: http://adni.loni.usc.edu/wp-content/uploads/how_to_apply/ADNI_Acknowledgement_List.pdf.

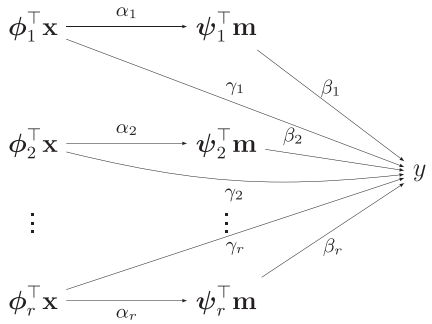

FIGURE 1 | A conceptual diagram with r parallel mediation paths. $\boldsymbol{\phi}_1^\top \mathbf{x}, \ldots, \boldsymbol{\phi}_r^\top \mathbf{x}$ are r orthogonal exposure components. $\boldsymbol{\psi}_j^\top \mathbf{m}$ is the mediator component associated with $\boldsymbol{\phi}_j^\top \mathbf{x}$, for $j = 1, \ldots, r$.

where Aβ is the main component of amyloid plaques and tau is the main component of neurofibrillary tangles. In AD pathophysiological models, it is hypothesized that Aβ and tau deposition can disrupt cell-to-cell communications and destroy brain cells, which leads to structural atrophy in areas such as the medial temporal lobe and ultimately deficits in cognitive functions [2]. The CSF contains proteins related to various biological processes. With high-throughput proteomics technology, many proteins have been consistently identified whose alterations are associated with AD. Among these, many have also been verified to be related to Aβ and/or tau pathology [3]. A stereotypical pattern of neurodegeneration suggests that brain atrophy occurs early in the medial temporal lobe and soon spreads to the rest of the cortical areas following the temporal–parietal–frontal trajectory, while motor areas are not generally impacted until later stages of AD [4]. Based on the pattern of intraneuronal neurofibrillary changes, Braak and Braak [5] characterized six stages and marked affected brain regions under each stage. For example, the entorhinal cortex (located in the medial temporal lobe) is a Braak I region affected by tau propagation first. In this study, we aim to expand the study scope by considering a data-driven approach to identify mechanisms of CSF protein alteration–brain atrophy–memory decline using CSF proteomics, brain volumetric, and memory behavior measurement data from ADNI. Meanwhile, rather than studying the considered features individually, it is expected that these features are grouped into components to better understand the interactions among features. We would also like to note that though inference on the mechanistic path effects is one objective, the identified components should be considered as an exploration on feature interactions.

Based on the biological assumptions, we formulate the problem as a mediation analysis with multiple exposures (intensity of CSF proteins/peptides), multiple mediators (volume of brain regions), and a continuous scalar outcome (measurement of memory behavior). Mediation analysis aims to delineate the underlying mechanism between the exposure and the outcome by decomposing the exposure effect into the part through the mediator (called the indirect effect) and the part not through the mediator (called the direct effect). Cases with a single exposure and a single mediator have been extensively studied (see a review by VanderWeele [6] and references therein) and various extensions for different data types, such as time-to-event data [7], time series [8], and functional data [9, 10], have been introduced. With the spread utilization of data acquired from high-throughput technologies, approaches for mediation analysis are adapted to dealing with high-dimensional mediators, where high-dimensional omics or neuroimaging data are considered as the mediator candidates aiming to identify significant biological mediation pathways (examples include Huang and Pan [11], Chen et al. [12], Song et al. [13], Zhao, Lindquist, and Caffo [14], Zhao and Luo [15], among many others). Approaches for both multiple exposures and multiple mediators are relatively sparse. In a recent work, Aung et al. [16] proposed to reduce the dimension of the exposures into a small number of groups based on prior domain knowledge and verified that the inter-group correlation is negligible. Long et al. [17] introduced a general framework for the case of multiple exposures, multivariate mediators, and various types of outcomes. Though correlations among exposures were allowed, it is assumed that the dependencies are fully captured via the observed confounders. When applied to the study with gene expression as the exposures, the principal component analysis (PCA) was firstly applied to the mRNA data. For the intermediate variable, only five metabolic proteins were preselected as potential mediators. For implementation, this approach requires the specification of exposure-to-mediator path to estimate the path effects. Zhou, Wang, and Zhao [18] proposed high-dimensional linear mediation analysis models and provided asymptotic guarantees for inference procedures under various settings including incomplete mediation and complete mediation. In the outcome model, a linear representation of the mediators and the exposures is correspondingly assumed. Under the proposed linear mediation models, the dissection of individual path effects becomes challenging and thus, the introduced inference procedure focuses on the total indirect effect. Zhang [19] developed two regularization procedures for a large number of exposures and mediators, but the procedures require the mediators to be independent, which is an overly stringent assumption for brain volumetric data. Recently, Zhao and Li [20] introduced a framework for high-dimensional exposures and high-dimensional mediators, which combines PCA with regularized mediation estimation for exposure and mediator selection. The PCA is applied to the exposures to create independent components, which can be considered a data processing step. One drawback of this approach is without considering the connections to the mediators and outcome when doing the PCA. In addition, with regularized estimators, the post-selection inference is not straightforward.

In mediation analysis, one popular parametric approach is the linear structural equation modeling (LSEM) framework. One example is the Baron and Kenny [21] approach, where two regression models are assumed, one for the mediator and one for the outcome. For a regression problem with multivariate dependent and multivariate independent variables, partial least squares (PLS) and its extensions are widely implemented. In a PLS regression, latent structures of the dependent and independent variables that demonstrate the strongest associations are identified. As a variance-based SEM technique, PLS has also been utilized in path modeling including mediation analysis [22]. Using the case of a single exposure and single mediator for demonstration, Nitzl, Roldan, and Cepeda [22] and Carrión, Nitzl, and Roldán [23] illustrated the state-or-the-art use of mediation analysis in the context of PLS-SEM, where a decision tree and classification of mediation effects were recommended. The authors also briefly discussed the handling of two mediators,

either competitive (parallel) or connected (dependent), using PLS path modeling. As mentioned in these literature, PLS can be a useful tool for advanced mediation analysis. However, more complex scenarios require further investigation. In this study, we adopt the idea of PLS to mediation analysis with multiple exposures and multiple mediators to identify orthogonal latent structures of the exposures and mediators that constitute parallel mediation mechanisms. This idea of assuming independent latent exposure and mediator components is also in line with existing PCA-based approaches aiming to create parallel mediation paths, where in high-dimensional mediation analysis, PCA was applied to the mediators [11, 14], and in the above-mentioned approaches for multiple exposures and multiple mediators, independent exposures were created via either PCA or using domain knowledge. No existing approach assumes latent structures on both exposures and mediators that constitute independent mediation paths. With multiple exposures and mediators, when the mediation paths are parallel, it greatly simplifies the problem as it can be handled separately by performing a series of marginal mediation analyses [24, 25]. For a mediation analysis, the LSEM framework has two regression models. Thus, different from a PLS regression, information contained in both regression models should be taken into consideration when identifying the latent structures and estimating the model parameters. As the exposures, mediators, and outcome are all assumed to be continuous variables in this study, by imposing normality assumptions, the joint likelihood function of the LSEMs is derived and estimators that maximize the joint likelihood function are introduced to identify the latent structures and effect parameters.

Compared to existing approaches, in our proposal, instead of assuming conditional independence among the exposures directly, it is assumed that there exist latent exposure factors that are (conditionally) independent and induce parallel mediation paths. Corresponding to each latent exposure factor, a latent mediator factor is assumed that mediates the exposure effect on the outcome, which allows the dependence among observed mediator variables. In addition, instead of selecting individual mediators using either a testing or a regularization approach, the identification of latent factors serves as a grouping procedure and enables a network-level interpretation, which may provide a better elucidation in some biological processes. For example, considering the ADNI proteomics-imaging study, a single protein does not function alone and impacts solely the atrophy level of one brain region. Rather, it is hypothesized that proteins interact with each other and together exert influence on the atrophy of multiple brain regions and ultimately cognitive behaviors. The proposed approach is designed to identify these groups of proteins and groups of brain regions. Compared to a recently introduced linear mediation model [18], instead of conducting inference on the total indirect effect, the proposed approach enables the identification of multiple parallel mediation paths and test for significant mediation effect of each path individually. This provides a better articulation of the underlying mechanisms. On the other hand, from a methodological perspective, the proposed approach introduces an integrative procedure of estimating all parameters together by optimizing the joint likelihood function of the exposures, mediators, and outcomes. On the contrary, most of the existing approaches yield estimation of the parameters via multiple steps. Some may even include data processing steps to create independent exposures and/or mediators. For those regularization-based approaches, such as the one introduced by Zhao and Li [20], conducting inference on the selected mediation paths is challenging. The proposed approach yields the goal of path selection via the identification of latent factors on both the exposures and mediators and meanwhile, offers inference on the path effects, which can be achieved via proceeding with a bootstrap procedure.

The rest of the manuscript is organized as the following. Section 2 introduces a mediation analysis approach for the scenario of multiple exposures and multiple mediators under the LSEM framework, where the multivariate data are projected into lower-dimensional spaces for mediation mechanisms. Likelihood-based estimators are introduced and an estimation algorithm is proposed for simultaneous identification of the projecting vectors and model coefficients. Asymptotic distribution of the estimators are derived under the lower-dimensional case. A bootstrap procedure is introduced for inference. In Section 3, simulation studies are presented to demonstrate the performance of the proposal. Section 4 applies the mediation framework to the ADNI proteomic-imaging study. A discussion on the identified proteins, brain regions, and mediation paths are included. Section 5 summarizes the manuscript with discussions.

2 | MODEL AND METHOD

For subject $i \in \{1, \dots, n\}$, where n is the number of subjects, let $\mathbf{x}_i = (x_{i1}, \dots, x_{ip})^\top \in \mathbb{R}^p$ denote the p-dimensional exposures, $\mathbf{m}_i = (m_{i1}, \dots, m_{iq})^\top \in \mathbb{R}^q$ denote the q-dimensional mediators, and $y_i \in \mathbb{R}$ denote the scalar outcome. Let $\mathbf{w}_i = (w_{i1}, \dots, w_{is})^\top \in \mathbb{R}^s$ denote the s-dimensional covariates (with the first element of one for the intercept). These can be pre-exposure covariates and/or post-exposure mediator-outcome confounding factors not induced by the exposures. In the ADNI application, $\mathbf{x}_i$ is the intensity of $p = 35$ CSF proteins, $\mathbf{m}_i$ is the brain volumetric data extracted from $q = 37$ regions of interest using an atlas by Doshi et al. [26], y_i is a composite memory score (ADNI_MEM) calculated from a battery of neuropsychological tests, and $\mathbf{w}_i$ includes age, gender, and years of education. Let $\mathbf{X} = (\mathbf{x}_1, \dots, \mathbf{x}_n)^\top \in \mathbb{R}^{n\times p}$, $\mathbf{M} = (\mathbf{m}_1, \dots, \mathbf{m}_n)^\top \in \mathbb{R}^{n\times q}$, $\mathbf{W} = (\mathbf{w}_1, \dots, \mathbf{w}_n)^\top \in \mathbb{R}^{n\times s}$, and $\mathbf{Y} = (y_1, \dots, y_n)^\top \in \mathbb{R}^n$. Let $r \le \min(p, q)$, it is assumed that the covariance of $\mathbf{x}_i$ and $\mathbf{m}_i$ has the following decomposition as $\mathrm{Cov}(\mathbf{x}_i) = \mathbf{\Phi}^\top\mathbf{\Delta}\mathbf{\Phi} + \mathbf{\Pi} = \sum_{j=1}^r \delta_j \boldsymbol{\phi}_j\boldsymbol{\phi}_j^\top + \mathbf{\Pi}$ and $\mathrm{Cov}(\mathbf{m}_i) = \mathbf{\Psi}^\top\mathbf{\Lambda}\mathbf{\Psi} + \mathbf{\Omega} = \sum_{j=1}^r \lambda_j \boldsymbol{\psi}_j\boldsymbol{\psi}_j^\top + \mathbf{\Omega}$, where $\mathbf{\Phi} = (\boldsymbol{\phi}_1, \dots, \boldsymbol{\phi}_r) \in \mathbb{R}^{p\times r}$ and $\mathbf{\Psi} = (\boldsymbol{\psi}_1, \dots, \boldsymbol{\psi}_r) \in \mathbb{R}^{q\times r}$ are orthonormal matrices such that $\mathbf{\Phi}^\top\mathbf{\Phi} = \mathbf{\Psi}^\top\mathbf{\Psi} = \mathbf{I}_r$, $\mathbf{\Delta} = \mathrm{diag}\{\delta_1, \dots, \delta_r\} \in \mathbb{R}^{r\times r}$ and $\mathbf{\Lambda} = \mathrm{diag}\{\lambda_1, \dots, \lambda_r\} \in \mathbb{R}^{r\times r}$ are diagonal matrices. $\mathbf{\Pi} \in \mathbb{R}^{p\times p}$ is of rank $(p - r)$ and orthogonal to $\mathbf{\Phi}^\top\mathbf{\Delta}\mathbf{\Phi}$, and $\mathbf{\Omega} \in \mathbb{R}^{q\times q}$ is of rank $(q - r)$ and orthogonal to $\mathbf{\Psi}^\top\mathbf{\Lambda}\mathbf{\Psi}$. For a pair of $\boldsymbol{\phi}_j$ and $\boldsymbol{\psi}_j$, the following linear structural equation models (LSEMs) are assumed.

$$\mathbf{M}\boldsymbol{\psi}_j = \mathbf{X}\boldsymbol{\phi}_j \cdot \alpha_j + \mathbf{W}\theta_{1j} + \boldsymbol{\varepsilon}_j, \quad j = 1, \dots, r \tag{1}$$

$$\mathbf{Y} = \sum_{j=1}^{r} \left(\mathbf{X}\boldsymbol{\phi}_j \cdot \gamma_j + \mathbf{M}\boldsymbol{\psi}_j \cdot \beta_j\right) + \mathbf{W}\theta_2 + \boldsymbol{\eta} \tag{2}$$

where $\{\alpha_j\}, \{\beta_j\}, \{\gamma_j\}, \{\theta_{1j} \in \mathbb{R}^s\}, \theta_2 \in \mathbb{R}^s$ are model coefficients, $\{\boldsymbol{\varepsilon}_j = (\varepsilon_{j1}, \dots, \varepsilon_{jn})^\top \in \mathbb{R}^n\}$ and $\boldsymbol{\eta} = (\eta_1, \dots, \eta_n)^\top \in \mathbb{R}^n$ are model

errors. $\boldsymbol{\varepsilon}_j$ is assumed to be independent of $\mathbf{X}$ and $\mathbf{W}$, and $\boldsymbol{\eta}$ is independent of $\mathbf{X}$, $\mathbf{M}$, and $\mathbf{W}$. Under the assumption that there exists no unmeasured mediator-outcome confounder, $\boldsymbol{\varepsilon}_j$ is independent of $\boldsymbol{\eta}$. For continuous outcome and mediator, it is assumed that the errors follow normal distributions, where ϵ_{ji} follows a normal distribution with mean zero and variance σ_j^2 and η_i follows a normal distribution with mean zero and variance τ^2.

Following the above definitions and Models (1) and (2), $\boldsymbol{\phi}_j^\top \mathbf{x}$, which is a linear projection of the exposure variables, is called an exposure component; and $\boldsymbol{\psi}_j^\top \mathbf{m}$, a linear projection of the mediator variables, is the associated mediator component. The models assume that for an exposure component, the associated mediator component captures the mediation effect on the outcome. In the ADNI application, CSF protein intensities are the exposures and brain volumetric data are the mediators. With proper thresholding or sparsifying, the projections identify a combination of proteins and brain regions enabling a network-level interpretation of the mediation mechanism. With multiple projection pairs of exposure and mediator, it is assumed that the mediation paths are parallel to each other. In other words, there is no interference among the exposure components or the mediator components (as demonstrated in Figure 1). Under this assumption, the path effects are parallel to each other, and one can fit LSEMs for each pair of component separately [25]. Following this property, in Section 2.1, an algorithm will be introduced to identify multiple components sequentially. Figure 1 presents a conceptual mechanistic diagram with r parallel mediation paths. In the figure, the confounding factors ($\mathbf{w}$) are removed to focus on the mediation mechanisms. Under the proposed models, $\mathrm{DE}(\boldsymbol{\phi}_j^\top \mathbf{x}) = \gamma_j$ is the direct effect of the jth exposure component on the outcome, $\mathrm{IE}(\boldsymbol{\phi}_j^\top \mathbf{x}, \boldsymbol{\psi}_j^\top \mathbf{m}) = \alpha_j \beta_j$ is the indirect effect of the jth exposure component on the outcome through the corresponding mediator component, and $\mathrm{TE}(\boldsymbol{\phi}_j^\top \mathbf{x}) = \mathrm{DE}(\boldsymbol{\phi}_j^\top \mathbf{x}) + \mathrm{IE}(\boldsymbol{\phi}_j^\top \mathbf{x}, \boldsymbol{\psi}_j^\top \mathbf{m}) = \gamma_j + \alpha_j \beta_j$ is the total effect of the jth exposure component. In Section A of the supporting informations, causal definitions under the potential outcome framework and assumptions for identification are discussed.

2.1 | Estimation

In Models (1) and (2), not only the model coefficients but also the projections need to be estimated. As discussed above, one can fit the models for each component pair separately under the parallel assumption. It is proposed to estimate the corresponding parameters sequentially. In the following, the estimation is focused on one pair of component and drop the component index j without confusion to keep the notations uncluttered. Let $\Theta = (\boldsymbol{\phi}, \boldsymbol{\psi}, \alpha, \beta, \gamma, \theta_1, \theta_2, \sigma^2, \tau^2)$ denote the parameter set. Under the normality assumption, it is proposed to estimate the parameters by minimizing the negative joint likelihood function given by the following (after removing the constant terms)

$$\ell(\Theta) = \frac{1}{\sigma^2}\|\mathbf{M}\boldsymbol{\psi} - \mathbf{X}\boldsymbol{\phi}\alpha - \mathbf{W}\theta_1\|_2^2 + \frac{1}{\tau^2}\|\mathbf{Y} - \mathbf{X}\boldsymbol{\phi}\gamma - \mathbf{M}\boldsymbol{\psi}\beta - \mathbf{W}\theta_2\|_2^2 + n\log\sigma^2 + n\log\tau^2 \tag{3}$$

Note that the parameters are not identifiable due to the existence of the products, $\boldsymbol{\phi}\alpha$, $\boldsymbol{\phi}\gamma$, and $\boldsymbol{\psi}\beta$. To uniquely estimate the parameters, it is imposed that $\boldsymbol{\phi}$ and $\boldsymbol{\psi}$ both have the vector norm of one. The objective function is then written as

$$\begin{aligned} &\text{minimize } \ell(\Theta), \\ &\text{such that } \|\boldsymbol{\phi}\|_2 = 1, \quad \|\boldsymbol{\psi}\|_2 = 1 \end{aligned} \tag{4}$$

It is easy to show that ℓ is biconvex over $(\boldsymbol{\phi}, \boldsymbol{\psi}, \alpha, \beta, \gamma, \theta_1, \theta_2, 1/\sigma^2, 1/\tau^2)$. Thus, it is proposed to estimate the parameters by (block) coordinate descent. In the following, we discuss the solution to each parameter. For $\boldsymbol{\phi}$, assuming $(\boldsymbol{\psi}, \alpha, \beta, \gamma, \theta_1, \theta_2, \sigma^2, \tau^2)$ is given, because of the constraint, the Lagrangian form is

$$\mathcal{L}(\boldsymbol{\phi}, \lambda_1) = \ell(\boldsymbol{\phi}) + \lambda_1(\boldsymbol{\phi}^\top\boldsymbol{\phi} - 1) \tag{5}$$

where λ_1 is the Lagrangian parameter. By taking partial derivatives and setting to zero,

$$\hat{\boldsymbol{\phi}} = \left\{\left(\frac{\alpha^2}{\sigma^2} + \frac{\gamma^2}{\tau^2}\right)\mathbf{X}^\top\mathbf{X} + \lambda_1\mathbf{I}\right\}^{-1} \underbrace{\mathbf{X}^\top\left\{\left(\frac{\alpha}{\sigma^2} - \frac{\beta\gamma}{\tau^2}\right)\mathbf{M}\boldsymbol{\psi} + \frac{\gamma}{\tau^2}\mathbf{Y} - \left(\frac{\alpha}{\sigma^2}\mathbf{W}\theta_1 + \frac{\gamma}{\tau^2}\mathbf{W}\theta_2\right)\right\}}_{\mathbf{U}} \tag{6}$$

and λ_1 is the solution to

$$\boldsymbol{\phi}^\top\boldsymbol{\phi} - 1 = \mathbf{U}^\top\left\{\left(\frac{\alpha^2}{\sigma^2} + \frac{\gamma^2}{\tau^2}\right)\mathbf{X}^\top\mathbf{X} + \lambda_1\mathbf{I}\right\}^{-2}\mathbf{U} - 1 = 0 \tag{7}$$

which can be solved by any algorithm that finds the unique root of a function. Analogously for $\boldsymbol{\psi}$ (given $\boldsymbol{\phi}, \alpha, \beta, \gamma, \theta_1, \theta_2, \sigma^2, \tau^2$), the solution is

$$\hat{\boldsymbol{\psi}} = \left\{\left(\frac{1}{\sigma^2} + \frac{\beta^2}{\tau^2}\right)\mathbf{M}^\top\mathbf{M} + \lambda_2\mathbf{I}\right\}^{-1} \underbrace{\mathbf{M}^\top\left\{\left(\frac{\alpha}{\sigma^2} - \frac{\beta\gamma}{\tau^2}\right)\mathbf{X}\boldsymbol{\phi} + \frac{\beta}{\tau^2}\mathbf{Y} + \left(\frac{1}{\sigma^2}\mathbf{W}\theta_1 - \frac{\beta}{\tau^2}\mathbf{W}\theta_2\right)\right\}}_{\mathbf{V}} \tag{8}$$

where λ_2 is the Lagrangian parameter and the value is the solution to

$$\boldsymbol{\psi}^\top\boldsymbol{\psi} - 1 = \mathbf{V}^\top\left\{\left(\frac{1}{\sigma^2} + \frac{\beta^2}{\tau^2}\right)\mathbf{M}^\top\mathbf{M} + \lambda_2\mathbf{I}\right\}^{-2}\mathbf{V} - 1 = 0 \tag{9}$$

For the model coefficients,

$$\begin{aligned} \hat{\alpha} &= (\boldsymbol{\phi}^\top\mathbf{X}^\top\mathbf{X}\boldsymbol{\phi})^{-1}(\boldsymbol{\phi}^\top\mathbf{X}^\top)(\mathbf{M}\boldsymbol{\psi} + \mathbf{W}\theta_1), \\ \hat{\beta} &= (\boldsymbol{\psi}^\top\mathbf{M}^\top\mathbf{M}\boldsymbol{\psi})^{-1}(\boldsymbol{\psi}^\top\mathbf{M}^\top)(\mathbf{Y} - \gamma\mathbf{X}\boldsymbol{\phi} - \mathbf{W}\theta_2), \\ \hat{\gamma} &= (\boldsymbol{\phi}^\top\mathbf{X}^\top\mathbf{X}\boldsymbol{\phi})^{-1}(\boldsymbol{\phi}^\top\mathbf{X}^\top)(\mathbf{Y} - \beta\mathbf{W}\boldsymbol{\psi} - \mathbf{W}\theta_2), \\ \hat{\theta}_1 &= (\mathbf{W}^\top\mathbf{W})^{-1}\mathbf{W}^\top(\mathbf{M}\boldsymbol{\psi} - \alpha\mathbf{X}\boldsymbol{\phi}), \\ \hat{\theta}_2 &= (\mathbf{W}^\top\mathbf{W})^{-1}\mathbf{W}^\top(\mathbf{Y} - \gamma\mathbf{X}\boldsymbol{\phi} - \beta\mathbf{M}\boldsymbol{\psi}) \end{aligned} \tag{10}$$

For the variances,

$$\begin{aligned} \hat{\sigma}^2 &= \frac{1}{n}\|\mathbf{M}\boldsymbol{\psi} - \mathbf{X}\boldsymbol{\phi}\alpha - \mathbf{W}\theta_1\|_2^2, \\ \hat{\tau}^2 &= \frac{1}{n}\|\mathbf{Y} - \mathbf{X}\boldsymbol{\phi}\gamma - \mathbf{M}\boldsymbol{\psi}\beta - \mathbf{W}\theta_2\|_2^2 \end{aligned} \tag{11}$$

Algorithm 1 summarizes the estimation procedure to simultaneously identify the first exposure and mediator component and

ALGORITHM 1 | The optimization algorithm for (4).

Input: $(\mathbf{X}, \mathbf{M}, \mathbf{W}, \mathbf{Y})$.

1: **initialization**: $\left\{\boldsymbol{\phi}^{(0)}, \boldsymbol{\psi}^{(0)}, \alpha^{(0)}, \beta^{(0)}, \gamma^{(0)}, \theta_1^{(0)}, \theta_2^{(0)}, \sigma^{2(0)}, \tau^{2(0)}\right\}$.

2: **repeat**

3: update $\boldsymbol{\phi}^{(s+1)}$ given $\boldsymbol{\psi}^{(s)}, \alpha^{(s)}, \beta^{(s)}, \gamma^{(s)}, \theta_1^{(s)}, \theta_2^{(s)}, \sigma^{2(s)}, \tau^{2(s)}$ by (6) and (7).

4: update $\boldsymbol{\psi}^{(s+1)}$ given $\boldsymbol{\phi}^{(s+1)}, \alpha^{(s)}, \beta^{(s)}, \gamma^{(s)}, \theta_1^{(s)}, \theta_2^{(s)}, \sigma^{2(s)}, \tau^{2(s)}$ by (8) and (9).

5: update $\alpha^{(s+1)}, \beta^{(s+1)}, \gamma^{(s+1)}, \theta_1^{(s+1)}, \theta_2^{(s+1)}$ given $\boldsymbol{\phi}^{(s+1)}, \boldsymbol{\psi}^{(s+1)}, \sigma^{2(s)}, \tau^{2(s)}$ by (10).

6: update $\sigma^{2(s+1)}, \tau^{2(s+1)}$ given $\boldsymbol{\phi}^{(s+1)}, \boldsymbol{\psi}^{(s+1)}, \alpha^{(s+1)}, \beta^{(s+1)}, \gamma^{(s+1)}, \theta_1^{(s+1)}, \theta_2^{(s+1)}$ by (11).

7: **until** the stopping criterion is met.

Output: $\left\{\hat{\boldsymbol{\phi}}, \hat{\boldsymbol{\psi}}, \hat{\alpha}, \hat{\beta}, \hat{\gamma}, \hat{\theta}_1, \hat{\theta}_2, \hat{\sigma}^2, \hat{\tau}^2\right\}$.

estimate the effect parameters. In the algorithm, the stopping criterion can be set as that the maximum absolute difference in the updates of model coefficients is less than a small value of $\varepsilon > 0$. In practice, occasions, such as $\boldsymbol{\phi}$ or $\boldsymbol{\psi}$ or both are prespecified, may occur. For example, the p exposures are mutually independent. For the jth exposure, one can specify $\boldsymbol{\phi}_j$ as a p-dimensional vector with the jth element one and the rest zero. Under these occasions, one can modify Algorithm 1 by setting the corresponding projection vector(s) to the prespecified value and optimizing over the rest parameters.

To identify higher-order components, as the orthogonality assumptions are imposed, it is proposed to remove the identified components from the data, similar to the identification of higher-order components in the principal component analysis. Let $\hat{\boldsymbol{\Phi}}^{(k)} = (\hat{\boldsymbol{\phi}}_1, \ldots, \hat{\boldsymbol{\phi}}_k) \in \mathbb{R}^{p\times k}$ and $\hat{\boldsymbol{\Psi}}^{(k)} = (\hat{\boldsymbol{\psi}}_1, \ldots, \hat{\boldsymbol{\psi}}_k) \in \mathbb{R}^{q\times k}$ denote the first k projections of the exposures and mediators, respectively. For $i = 1, \ldots, n$, let

$$\hat{\mathbf{x}}_i^{(k+1)} = \mathbf{x}_i - \mathbf{x}_i\hat{\boldsymbol{\Phi}}^{(k)}\hat{\boldsymbol{\Phi}}^{(k)\top} \quad \text{and} \quad \hat{\mathbf{m}}_i^{(k+1)} = \mathbf{m}_i - \mathbf{m}_i\hat{\boldsymbol{\Psi}}^{(k)}\hat{\boldsymbol{\Psi}}^{(k)\top} \tag{12}$$

be the new exposure and mediator, respectively. As the parallel assumption is imposed on the mediation paths, the effects from the identified components should be removed from the outcome making the next mediation mechanism orthogonal to the existing ones. Let $\{\hat{\gamma}_j\}_{j=1}^k$ and $\{\hat{\beta}_j\}_{j=1}^k$ denote the estimated model coefficients in (2) of the first k components. For $i = 1, \ldots, n$, let

$$\hat{y}_i^{(k+1)} = y_i - \sum_{j=1}^{k}(\hat{\boldsymbol{\phi}}_j^\top\mathbf{x}_i)\hat{\gamma}_j - \sum_{j=1}^{k}(\hat{\boldsymbol{\psi}}_j^\top\mathbf{m}_i)\hat{\beta}_j \tag{13}$$

be the new outcome. Applying Algorithm 1 to the new data, $\{\hat{\mathbf{x}}_i^{(k+1)}, \hat{\mathbf{m}}_i^{(k+1)}, \hat{y}_i^{(k+1)}, \mathbf{w}_i\}$, one can identify the $(k+1)$th component of $\boldsymbol{\phi}$ and $\boldsymbol{\psi}$, which are orthogonal to $\hat{\boldsymbol{\Phi}}^{(k)}$ and $\hat{\boldsymbol{\Psi}}^{(k)}$, respectively. By transforming the data via removing the identified components from the exposure and mediator using (12) and the effects of these components from the outcome using (13), rather than imposing orthogonality constraints, the computational efficiency is significantly improved, especially when the dimensions are large. To determine the number of components, we propose to choose the number based on the significance of the indirect effect. Following the proposed algorithm, the components are identified sequentially based on the goodness-of-fit to the joint likelihood criterion; that is the first component fits the model the best yielding the highest value of the joint likelihood. The next component will yield the highest value of the joint likelihood on the transformed data after removing the first component; and so on for the following components. As one primary goal of mediation analysis is to identify paths with a nonzero mediation effect, the procedure terminates when a component with an insignificant mediation effect appears. This procedure of data transformation and identifying components sequentially can be considered as an analogy to the estimation procedure of PCA and canonical correlation analysis. In Section 2.3, a bootstrap approach is proposed to draw inference on the direct and indirect effects. As in most cases, the study interest is in the indirect effect, the number of components can be then chosen as the first r components with a significant indirect effect.

2.2 | Asymptotic Properties

In this section, the asymptotic properties of the proposed estimators are discussed under the scenario that $p, q \ll n$ and p, q are fixed. As normality is assumed and the proposed estimators are maximum likelihood estimators, likelihood-based asymptotic theories can be applied. The following theorem, Theorem 1, gives the asymptotic distribution of the proposed estimators.

Theorem 1. *Let* $\Theta = \{\boldsymbol{\phi}, \boldsymbol{\psi}, \alpha, \beta, \gamma, \theta_1, \theta_2\}$. *For* $p, q \ll n$ *and fixed, assume that as* $n \to \infty$, $\mathbf{X}^\top\mathbf{X}/n \to \mathbf{P} \in \mathbb{R}^{p\times p}$, $\mathbf{M}^\top\mathbf{M}/n \to \mathbf{Q} \in \mathbb{R}^{q\times q}$, $\mathbf{X}^\top\mathbf{M}/n \to \mathbf{R} \in \mathbb{R}^{p\times q}$, $\boldsymbol{\phi}^\top\mathbf{X}^\top\mathbf{X}\boldsymbol{\phi}/n \to \kappa_x$, $\boldsymbol{\psi}^\top\mathbf{M}^\top\mathbf{M}\boldsymbol{\psi}/n \to \kappa_m$, $\boldsymbol{\phi}^\top\mathbf{X}^\top\mathbf{M}\boldsymbol{\psi}/n \to \kappa_{xm}$, $\mathbf{W}^\top\mathbf{W}/n \to \mathbf{S} \in \mathbb{R}^{s\times s}$, $\mathbf{X}^\top\mathbf{W}/n \to \mathbf{U} \in \mathbb{R}^{p\times s}$ *and* $\mathbf{M}^\top\mathbf{W}/n \to \mathbf{V} \in \mathbb{R}^{q\times s}$. *Under Models* (1) *and* (2) *and normally distributed errors, the estimators proposed in Section* 2.1 *have the following asymptotic distributions.*

$$\sqrt{n}(\hat{\Theta} - \Theta) \xrightarrow{D} \mathcal{N}(\mathbf{0}, \tilde{\mathrm{I}}^{-1}(\Theta)) \tag{14}$$

where $\tilde{\mathrm{I}}(\Theta)$ *is provided in Section* B.1 *of the supporting informations.*

2.3 | Inference

Theorem 1 offers the asymptotic distribution of the proposed estimators for the parameters in the LSEMs. For the indirect effect, denoted as the product of α and β, inference based on the asymptotic results can be derived using the Delta method [27]. However, considering the fact that in finite sample, the distribution of $\hat{\alpha}_j\hat{\beta}_j$ can be far from Gaussian, a nonparametric bootstrap procedure is proposed to perform inference on the direct and indirect effects. The following gives the steps for the jth component. It should be noted that the following procedure is implemented by fixing $(\hat{\boldsymbol{\phi}}_j, \hat{\boldsymbol{\psi}}_j)$ estimated from the full dataset. Uncertainty in estimating these projections is not taken into consideration as the focus is on the inference of the path effects. To perform inference on $(\hat{\boldsymbol{\phi}}_j, \hat{\boldsymbol{\psi}}_j)$ via a bootstrap procedure, it encounters challenges of sign ambiguity and matching/reordering of the projections across bootstrap samples. The inference performance will then highly depends on the quality of the matching step and the metrics used for matching. Besides, including the estimation and matching of $(\boldsymbol{\phi}_j, \boldsymbol{\psi}_j)$

will significantly inflate the computation cost. We leave a rigorous study of the inference on the projection vectors to future research.

Step 1. Generate a bootstrap sample $\{(\hat{\boldsymbol{\phi}}_j^\top \mathbf{x}_i)^*, (\hat{\boldsymbol{\psi}}_j^\top \mathbf{m}_i)^*, \mathbf{w}_i^*, y_i^*\}$ of size n by sampling with replacement.

Step 2. Estimate the model coefficients and variances using Algorithm 1 with $(\hat{\boldsymbol{\phi}}_j, \hat{\boldsymbol{\psi}}_j)$ known.

Step 3. Repeat Steps 1 and 2 for B times.

Step 4. Construct bootstrap confidence intervals for the direct and indirect effects using either the percentile or bias-corrected approach [28] under a pre-specified significance level.

3 | SIMULATION STUDY

We first use simulation studies to examine the performance of the proposed framework, named PCMA (principal component mediation analysis). Two competing approaches are considered for comparison. (1) As existing approaches for mediation analysis with multiple exposures and multiple mediators are scarce, this approach is derived from the PCA-based high-dimensional mediation analysis introduced by Huang and Pan [11] and named PCA-HP. It includes two steps: (i) conduct PCA on the exposures and treat top PCs accounting for at least 85% of the data variation as the independent exposures; (ii) for each exposure component, apply the approach in Huang and Pan [11] and test for significant mediator components. (2) An approach for multiple exposures and multivariate mediators [17] is implemented using the R package mediateR (named as mediateR). This approach requires the specification of exposure-to-mediator path and the true path is specified in the simulation.

In the study, $r = 2$ parallel mediation paths are considered to be significant. The exposures, $\mathbf{x}$, are generated from a multivariate normal distribution with mean zero and covariance matrix $\boldsymbol{\Sigma}_x$. $\boldsymbol{\Sigma}_x$ has the eigendecomposition of $\boldsymbol{\Sigma}_x = \boldsymbol{\Phi}\boldsymbol{\Lambda}\boldsymbol{\Phi}^\top$, where $\boldsymbol{\Phi} \in \mathbb{R}^{p\times p}$ is an orthonormal matrix and $\boldsymbol{\Lambda} \in \mathbb{R}^{p\times p}$ is a diagonal matrix with eigenvalues exponentially decay. The mediators, $\mathbf{m}$, are assumed to follow a multivariate normal distribution with covariance matrix $\boldsymbol{\Sigma}_m$, where $\boldsymbol{\Sigma}_m = \boldsymbol{\Psi}\boldsymbol{\Delta}\boldsymbol{\Psi}^\top$ with $\boldsymbol{\Sigma} \in \mathbb{R}^{q\times q}$ an orthonormal matrix and $\boldsymbol{\Delta} \in \mathbb{R}^{q\times q}$ a diagonal matrix. To generate $\mathbf{m}$, the PCs of $\mathbf{m}$ (denoted as $\tilde{\mathbf{m}}$) are generated first and then transform back as $\mathbf{m} = \boldsymbol{\Phi}\tilde{\mathbf{m}}$. The first two PCs are generated following model (1), where ε's are from the standard normal distribution, and the rest are normally distributed with mean zero and variance as the corresponding eigenvalue. The outcome, y, is generated following model (2) by adding up the two mediation paths. The model error, η, is from the standard normal distribution. For the two mediation paths, $(\alpha_1, \beta_1, \gamma_1) = (2, 2, 1)$ and $(\alpha_2, \beta_2, \gamma_2) = (2, 1, -1)$, thus $(\mathrm{IE}_1, \mathrm{DE}_1) = (4, 1)$ and $(\mathrm{IE}_2, \mathrm{DE}_2) = (2, -1)$. In this simulation study, for demonstration purposes, covariates are not considered. In practice, one can either include covariates in the models or treat covariate adjustment as a data processing step to remove the confounding effects [29]. Two scenarios of data dimension are considered: (1) $p = 5, q = 10$ and (2) $p = 35, q = 37$ (the same as the ADNI dataset in Section 4). To evaluate the performance, the following metrics are considered. For the projection vectors, the magnitude of the inner products, denoted as $|\langle\hat{\boldsymbol{\phi}}, \boldsymbol{\phi}\rangle|$ and $|\langle\hat{\boldsymbol{\psi}}, \boldsymbol{\psi}\rangle|$, is introduced as a similarity metric between the estimate and truth (ranging between zero and one since the projection vectors are of unit norm). A frequency of successfully identifying the components is reported, where a success is defined when the average of the two magnitudes is greater than 0.5. For the direct effect (DE) and indirect effect (IE), estimation bias, standard error (SE), and mean squared error (MSE) are reported. Simulations are repeated 200 times. For the mediateR approach, the model settings are different, where no projection is assumed. The estimated direct and indirect effects from the exposures are presented.

Table 1 presents the simulation results of estimating the direct effect (DE) and indirect effect (IE). For both scenarios, the proposed PCMA approach correctly identifies the two components 100% of the time. The PCA-HP approach only identifies the first component (C1) in scenario (1) and the percentage of identifying the target components is less than 100% in most of the cases. For scenario (1), the similarity of $\boldsymbol{\phi}$ and $\boldsymbol{\psi}$ estimates are both high over 0.900 using the PCMA approach. While the similarity of $\boldsymbol{\psi}$ estimate using the PCA-HP approach is around 0.600 and an increase in the sample size does not improve the performance. When the data dimension increases to $p = 35$ and $q = 37$, the similarity of $\boldsymbol{\phi}$ and $\boldsymbol{\psi}$ estimates from the PCMA approach is lower at the sample size of $n = 135$. When the sample size increases to $n = 500$, the performance of the PCMA approach significantly improves with similarities over 0.900. When comparing the SE of the similarities, the PCMA approach is much lower suggesting a more stable performance in identifying the components. For both scenarios, when comparing the performance in estimating the effects, the performance of the PCMA approach is superior with a lower bias, SE, and MSE and a higher power with 1000 bootstrap samples for inference, especially when the data dimension increases to $(p, q) = (35, 37)$. Figure C.1 in Section C.1 of the supporting informations presents the histogram and density plot of the estimated DE and IE over 200 replications. From the figure, the skewness of PCA-HP estimates is higher and the estimates are further away from the truth compared to the distributions and estimates from the proposed PCMA approach. Table 1 also presents the results from the mediateR approach. As the model settings are different, the estimated DE and IE are biased with a higher MSE. In addition, as the sample size increases, the MSE does not decrease. Section C.2 demonstrates the effectiveness of the proposed procedure (Section 2.1) in choosing the number of mediating components. Sections C.3 and C.4 examine the robustness of the PCMA approach to the violation of model assumptions, including the existence of unmeasured mediator-outcome confounding and model misspecification. For both cases, PCMA approach correctly identifies the mediating components, while the estimated effects may be biased (see more details in corresponding sections). The current simulation study considers low-dimensional scenarios. When the data dimension increases to be comparable with the sample size, the proposed PCMA approach fails and is unable to correctly identify the projections (see Section C.5 of the supporting informations).

4 | THE PROTEOMICS-IMAGING STUDY OF AD

In this section, the proposed approach is applied to a proteomic-imaging dataset from the ADNI study. The CSF proteomics data

TABLE 1 | Simulation results from 200 replicates.

							DE				IE			
(p, q)	n	Method		%	$\lvert\langle\hat{\phi}, \phi\rangle\rvert$ (SE)	$\lvert\langle\hat{\psi}, \psi\rangle\rvert$ (SE)	Bias	SE	MSE	Power	Bias	SE	MSE	Power
			C1	57%	0.998 (0.002)	0.633 (0.096)	2.357	0.540	5.846	1.000	−2.372	0.540	5.918	1.000
		PCA-HP	C2	0%	—	—	—	—	—	—	—	—	—	—
			C1	—	—	—	−0.847	0.222	0.767	0.095	−4.577	0.148	20.967	0.990
		mediateR	C2	—	—	—	0.807	0.434	0.839	0.075	−1.953	0.030	3.814	0.275
			C1	100%	0.930 (0.055)	0.969 (0.005)	−0.228	0.292	0.137	0.815	0.629	0.408	0.562	1.000
	100	PCMA	C2	100%	0.946 (0.041)	0.943 (0.017)	−0.230	0.231	0.106	1.000	−0.815	0.222	0.713	1.000
			C1	68%	0.999 (0.001)	0.622 (0.085)	2.414	0.447	6.026	1.000	−2.420	0.448	6.053	1.000
		PCA-HP	C2	0%	—	—	—	—	—	—	—	—	—	—
			C1	—	—	—	−0.842	0.099	0.719	0.410	−4.576	0.063	20.943	1.000
		mediateR	C2	—	—	—	0.806	0.159	0.674	0.140	−1.949	0.014	3.799	0.980
			C1	100%	0.967 (0.014)	0.976 (0.001)	−0.212	0.108	0.057	1.000	0.381	0.135	0.163	1.000
(5, 10)	500	PCMA	C2	100%	0.969 (0.015)	0.971 (0.003)	−0.202	0.099	0.051	1.000	−0.844	0.095	0.722	1.000
			C1	96%	0.899 (0.082)	0.855 (0.104)	0.039	0.876	0.765	0.440	−0.589	0.967	1.278	0.927
		PCA-HP	C2	100%	0.843 (0.098)	0.904 (0.092)	0.952	0.588	1.251	0.020	−1.003	1.301	2.691	0.195
			C1	—	—	—	−0.901	0.320	0.914	0.000	−3.938	0.072	15.517	0.000
		mediateR	C2	—	—	—	0.927	0.444	1.056	0.000	−2.073	0.059	4.301	0.000
			C1	100%	0.785 (0.068)	0.893 (0.022)	−0.300	0.441	0.283	0.665	1.711	0.741	3.474	1.000
	135	PCMA	C2	100%	0.751 (0.073)	0.695 (0.055)	−1.057	0.486	.1353	0.985	0.042	0.482	0.233	0.985
			C1	90%	0.968 (0.033)	0.878 (0.102)	0.337	0.824	0.789	0.878	−0.479	0.822	0.901	1.000
		PCA-HP	C2	99%	0.943 (0.046)	0.943 (0.074)	0.773	0.237	0.654	0.000	−0.850	0.851	1.443	0.187
			C1	—	—	—	−0.891	0.133	0.812	0.210	−3.938	0.025	15.509	0.700
		mediateR	C2	—	—	—	0.936	0.164	0.903	0.045	−2.064	0.021	4.260	0.905
			C1	100%	0.920 (0.024)	0.960 (0.005)	−0.198	0.129	0.056	1.000	0.637	0.181	0.438	1.000
(35, 37)	500	PCMA	C2	100%	0.930 (0.019)	0.911 (0.018)	−0.315	0.111	0.112	1.000	−0.699	0.110	0.501	1.000

Abbreviations: %, percentage of identifying the corresponding component; C1/C2, the two components with a significant mediation effect; DE, direct effect; IE, indirect effect; MSE, mean squared error; SE, standard error.

were acquired from targeted liquid chromatography multiple reaction monitoring mass spectrometry (LC/MS-MRM). MRM is a highly specific, sensitive, and reproducible label-free technique for targeted protein quantification. The objective of the original study is to examine the ability of a panel of MS-measured peptides in discriminating disease status. The list was selected based on their detection record in CSF and relevance to AD. These compounds were sent to the detector and went through a series of processing procedures, including peak integration, outliers detection, normalization, quantification, and quality control using test/retest samples. The intensity of a list of $p = 35$ proteins is considered as the exposures ($\mathbf{X}$) based on existing findings of AD proteomics studies [3]. A brain imaging measure obtained from anatomical magnetic resonance imaging (MRI) is considered as the mediator ($\mathbf{M}$). After following standard data preprocessing steps, volumetric measures from $q = 37$ regions of interest spanning the whole brain [26] were extracted. To adjust for variations in individual brain size, the volume of each brain region is standardized by the total intracranial volume. A cognitive outcome, called ADNI-MEM, is considered as the outcome variable (Y). It is a composite memory score calculated from a battery of neuropsychological tests. Covariates considered include age, gender, and years of education ($\mathbf{W}$). In this study, data from $n = 135$ subjects diagnosed with mild cognitive impairment (MCI) at recruitment are analyzed. As a prodromal stage of AD, subjects with MCI experience a slight but noticeable and measurable cognitive decline and an increased risk of developing AD or other types of dementia. Thus, understanding the disease pathology of MCI plays a key role in guiding early diagnosis and intervention for AD.

The proposed approach identifies three orthogonal components with a significant indirect effect, denoted as C1, C2, and C3. Table 2 presents the estimates and 95% confidence intervals from 1000 bootstrap samples. The indirect effect of all three components are significant and negative, while the underlying mechanism varies. In C1, α is significantly positive and β is significantly negative; in C2 and C3, α is significantly negative and β is significantly positive. For C1, as the intensity of the protein component increases, the volume of the corresponding brain component becomes relatively larger, while leading to a decrease in the memory score. For C2 and C3, it is the opposite that as the protein intensity increases, the brain volume decreases, leading to a memory decline. In order to better interpret the exposure

TABLE 2 | The estimates, standard error (SE), and 95% bootstrap confidence interval (CI) from 1000 samples of the model coefficients (α and β), indirect effect (IE), and direct effect (DE) of the three identified components.

	C1			C2			C3		
	Estimate	**SE**	**95% CI**	**Estimate**	**SE**	**95% CI**	**Estimate**	**SE**	**95% CI**
α	1.218	0.070	(1.083, 1.352)	−1.052	0.052	(−1.156, −0.957)	−1.110	0.057	(−1.224, −0.998)
β	−0.807	0.163	(−1.134, −0.497)	0.569	0.167	(0.247, 0.894)	0.946	0.200	(0.569, 1.340)
IE	−0.984	0.213	(−1.416, −0.588)	−0.600	0.184	(−0.971, −0.259)	−1.051	0.231	(−1.524, −0.622)
DE	1.878	0.231	(1.456, 2.345)	0.844	0.209	(0.438, 1.253)	1.245	0.292	(0.682, 1.818)

TABLE 3 | Proteins with top loading magnitude of the three components with a significant indirect effect. (Direction: Protein regulation direction in MCI/AD in existing literature.)

	Positive loading				Negative loading			
	Protein	**Loading**	**Gene**	**Direction**	**Protein**	**Loading**	**Gene**	**Direction**
C1	Neuronal pentraxin-2	0.358	NPTX2	↓	ProSAAS	−0.297	PCSK1N	⇳
	Neuronal cell adhesion molecule	0.358	NRCAM	⇳	Beta-2-microglobulin	−0.284	B2M	⇳
	Neurexin-1	0.341	NRXN1	↓	Chitinase-3-like protein 1	−0.268	CH3L1	↑
	Neurosecretory protein VGF	0.318	VGF	↓	Kallikrein-6	−0.205	KLK6	↑
	Prostaglandin-H2 D-isomerase	0.235	PTGDS	↓				
	Alpha-1B-glycoprotein	0.165	A1BG	⇳				
	Calsyntenin-3	0.152	CSTN3	⇳				
C2	Kallikrein-6	0.533	KLK6	↑	Brain acid soluble protein 1	−0.287	BASP1	⇳
	Clusterin	0.405	CLUS	⇳	Alpha-1B-glycoprotein	−0.277	A1BG	⇳
	Insulin-like growth factor-binding protein 2	0.225	IGFBP2	⇳	Apolipoprotein D	−0.229	APOD	⇳
					Apolipoprotein E	−0.229	APOE	⇳
					Glial fibrillary acidic protein	−0.189	GFAP	↑
	ProSAAS	0.420	PCSK1N	⇳	Alpha-1B-glycoprotein	−0.347	A1BG	⇳
	Prostaglandin-H2 D-isomerase	0.293	PTGDS	↓	Beta-2-microglobulin	−0.212	B2M	⇳
C3	Monocyte differentiation antigen CD14	0.243	CD14	↑	Mimecan	−0.197	OGN	⇳
	Compliment factor B	0.243	CFB	↑	Neurosecretory protein VGF	−0.185	VGF	↓
	Neuronal pentraxin-1	0.242	NPTX1	↓	Ectonucleotide pyrophosphatase/phosphodilesterase family member 2	−0.181	ENPP2	↑
	Calsyntenin-3	0.196	CSTN3	⇳	Chromogranin-A	−0.178	CHGA	⇳
	Complement C4-A	0.183	C4A	↑	Cystatin-C	−0.176	CST3	⇳
					Gamma-enolase	−0.176	ENO2	⇳

Abbreviations: ↑/↓, consistently upregulated/downregulated in MCI/AD; ⇳, inconsistent reports.

and mediator components, an *ad hoc* procedure is employed to sparsify the loading profile using the lasso regularization [30], similar to the sparse principal component analysis approach [31]. With the sparse loading profiles, each exposure and mediator component can be interpreted as a protein and brain network, respectively, that demonstrates a nonzero path effect on memory decline. Table 3 lists the top-loaded proteins in the components and Table 4 presents the top-loaded brain regions. These identified components offer a network-level interpretation on both the protein abundance (exposures) and brain atrophy (mediators) and suggest that within each component, proteins with a nonzero loading function together to impact the severity of atrophy on the corresponding nonzero-loaded mediator brain regions, which further leads to memory decline in these MCI subjects.

TABLE 4 | Brain regions with top loading magnitude of the three identified components with a significant indirect effect.

	Positive loading			Negative loading		
	Region	**Module**	**Loading**	**Region**	**Module**	**Loading**
C1	Frontal opercular (L)	Frontal	0.474	Ventricle (L)	Ventricle	−0.470
	Frontal inferior (L)	Frontal	0.319	Frontal medial (L)	Frontal	−0.371
	Temporal supratemporal (R)	Temporal	0.189	Ventricle (R)	Ventricle	−0.293
	Frontal insular (L)	Frontal	0.168	Cerebellum (R)	Cerebellum	−0.214
	Occipital lateral (R)	Occipital	0.135	Corpus callosum	Corpus callosum	−0.194
	Temporal lateral (R)	Temporal	0.107	Frontal lateral (L)	Frontal	−0.125
	Occipital medial (L)	Occipital	0.101			
	Occipital medial (R)	Occipital	0.241	Ventricle (R)	Ventricle	−0.466
	Frontal insular (R)	Frontal	0.234	Ventricle (L)	Ventricle	−0.408
	Frontal lateral (R)	Frontal	0.233	Temporal supratemporal (L)	Temporal	−0.277
	Occipital medial (L)	Occipital	0.179	Parietal lateral (L)	Parietal	−0.242
	Frontal medial (L)	Frontal	0.135	Parietal medial (R)	Parietal	−0.232
	Frontal opercular (L)	Frontal	0.135	Occipital lateral (R)	Occipital	−0.205
				Occipital inferior (R)	Occipital	−0.185
				Parietal medial (L)	Parietal	−0.159
				Frontal insular (L)	Frontal	−0.135
				Frontal lateral (L)	Frontal	−0.135
				Limbic medial temporal (R)	Limbic	−0.101
C2	Parietal medial (R)	Parietal	0.476	Frontal medial (L)	Frontal	−0.384
	Temporal lateral (L)	Temporal	0.277	Limbic cingulate (R)	Limbic	−0.322
	Limbic medial temporal (L)	Limbic	0.247	Temporal inferior (R)	Temporal	−0.228
	Limbic cingulate (L)	Limbic	0.221	Frontal inferior (L)	Frontal	−0.180
	Occipital lateral (R)	Occipital	0.218	Frontal opercular (R)	Frontal	−0.156
	Occipital lateral (L)	Occipital	0.171	Temporal lateral (R)	Temporal	−0.147
	Parietal lateral (R)	Parietal	0.157	Parietal medial (L)	Parietal	−0.134
				Occipital medial (R)	Occipital	−0.131
C3				Frontal insular (L)	Frontal	−0.115

Abbreviations: GM, gray matter; L, Left; R, Right; WM, white matter.

To better understand the functions of the proteins, in Table 3, the direction of protein level in MCI/AD compared to normal control reported in the existing literature is summarized. From the table, the sign of the loadings are in line with the (consistent) directions in C1 and mostly consistent in C2 and C3. For example, in C1, proteins with a positive loading are downregulated in MCI/AD and proteins with a negative loading are upregulated. As Aβ and tau are two primary protein markers for AD, we discuss the identified protein components based on the relevance to these two proteins. C1 and C3 can be primarily considered as Aβ pathological components, where NPTX2, PTGDS, VGF and CH3L1 in C1 and NPTX1, PTGDS, ENPP2, CST3, and CHGA are known to be related to Aβ pathology [32–36]. C2 is a component primarily relevant to tau pathology, where KLK6, IGFBP2, APOE and APOD are found tau-associated proteins in AD pathology [37–40] Many of these proteins were found to be related to brain regional atrophy. For example, NPTX1 and NPTX2 were found to be related to hippocampal volume and cognitive decline among AD patients [34]. Human KLK6 is primarily abundant in the spinal cord, brain stem, hippocampus, and thalamus [39, 41].

Table 4 presents the top-loaded brain regions in the identified components. Figure 2 shows these regions in a brain map. From the brain maps, the three components represent different portions of the brain suggesting three different brain mechanisms to memory decline. C1 is primarily the left prefrontal and medial lobe, the right temporal lobe, and the lateral ventricles. C2 is primarily the prefrontal and occipital medial lobe, as well as the lateral ventricles, on both hemispheres. C3 is primarily the temporal, medial, and occipital lobe on both hemispheres. Many covered regions in these three components were previously identified as marker regions with more severe atrophy in AD patients and are associated with memory deficits [4, 42–46]. Especially, the entorhinal and hippocampal atrophy are two well established and validated AD markers repeatedly reported in the existing literature. The entorhinal cortex was found to be affected by tau propagation first [5]. As a major component of

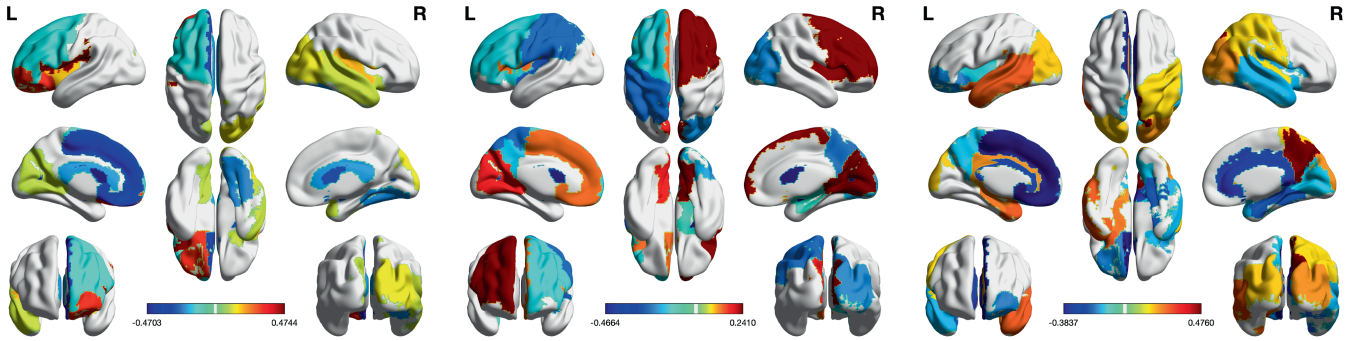

(a) C1 **(b)** C2 **(c)** C3

FIGURE 2 | The brain map of the three identified components with a significant indirect effect. (a) C1, (b) C2, (c) C3.

the medial temporal lobe, the hippocampus involves in functions including response inhibition, episodic memory, and spatial cognition [47]. Because of the sharp contrast between the CSF in the ventricles and surrounding tissues in brain structural images, volumetric measurement of the ventricles is robust to automatic segmentation. Enlargement in the ventricles is thus often considered a measurement of hemispheric atrophy rates and is consistently reported as an AD marker [48, 49].

In summary, the top-loaded features in the identified protein and brain components, as well as the direction of the effects, are in line with existing knowledge about AD. In addition, the proposed approach groups relevant features together offering a network-level interpretation and provides a mechanistic protein–imaging–cognition path illustration on memory deficits.

5 | DISCUSSION

In this study, a linear structural equation modeling framework is proposed for mediation analysis with multiple exposures and multiple mediators. The framework assumes that there exist underlying orthogonal mediation mechanisms on the outcome, thus named principal component mediation analysis (PCMA). Under the normality assumption, a likelihood-based approach is proposed to simultaneously estimate the orthogonal projections and effect parameters. Under a low-dimensional scenario, the asymptotic distributions of the proposed estimators are derived. A bootstrap procedure is also introduced for finite sample inference. Simulation studies demonstrate the superior performance of the proposal compared to a competing approach. In the ADNI proteomic-imaging study, the proposed approach identifies protein–brain structure components that have a significant mediation effect on memory decline among MCI patients. Features in the components are consistent with existing knowledge about AD and suggest pathological paths of CSF protein deposition–brain atrophy–memory deficit.

It should be noted that the ordering of the exposures and mediators in the AD study is determined based on biological mechanistic assumptions and current understanding of AD pathology. The findings should not be overinterpreted with causal relationships. In Section A of the supporting informations, casual assumptions are discussed. The proposed framework can also be used to integrate other types of multiview data, such as an imaging-genetics study, where the genetic data are the exposures and the neuroimaging data are the mediators, and integrating structural imaging data (exposures) and functional imaging data (mediators) based on Hebb's law [50]. One can also apply the proposed framework to longitudinal data where the causality is intrinsically inferred by the temporal ordering.

The proposed framework assumes the existence of latent components that connect the exposures, mediators, and outcome. The identified components are linear combinations of the exposure/mediator features making the interpretation less feasible. Though an *ad hoc* approach is suggested to sparsify the loading profiles, integrated approaches can be a future direction. This type of approach may also apply to the scenario of high-dimensional exposures and/or high-dimensional mediators. In the current study, asymptotic properties are derived under the low-dimensional scenario. Asymptotic theories under the high-dimensional setting are challenging without any constraint or regularization and thus are left to future research. The proposed estimators are likelihood-based estimators. In practice, when properly scaling the data and imposing unit variances ($\sigma = \tau = 1$), it is equivalent to the least squares estimation. The consistency still holds but the estimators are more robust to non-Gaussian continuous distributions [51, 52]. For other types of data outcome, such as a binary outcome, extensions to the generalized SEMs are feasible but require further investigation. The proposed framework assumes no interaction between the exposures and mediators. With multiple exposures and mediators, an extension of including interactions is not straightforward and is considered a future direction.

Acknowledgments

Yi Zhao was supported in part by NIH grants R01MH126970, P30AG 072976, and U54AG065181.

Conflicts of Interest

The authors declare no conflicts of interest.

Data Availability Statement

The data that support the findings of this study are openly available in the Alzheimer's disease neuroimaging initiative at https://adni.loni.usc.edu/about/.

References

1. J. Wiley, "Alzheimer's Disease Facts and Figures," *Alzheimer's & Dementia* 17 (2021): 327–406.

2. E. Mormino, J. Kluth, C. Madison, et al., "Episodic Memory Loss Is Related to Hippocampal-Mediated β-Amyloid Deposition in Elderly Subjects," *Brain* 132, no. 5 (2009): 1310–1323.

3. K. E. Wesenhagen, C. E. Teunissen, P. J. Visser, and B. M. Tijms, "Cerebrospinal Fluid Proteomics and Biological Heterogeneity in Alzheimer's Disease: A Literature Review," *Critical Reviews in Clinical Laboratory Sciences* 57, no. 2 (2020): 86–98.

4. L. Pini, M. Pievani, M. Bocchetta, et al., "Brain Atrophy in Alzheimer's Disease and Aging," *Ageing Research Reviews* 30 (2016): 25–48.

5. H. Braak and E. Braak, "Neuropathological Stageing of Alzheimer-Related Changes," *Acta Neuropathologica* 82, no. 4 (1991): 239–259.

6. T. J. VanderWeele, "Mediation Analysis: A Practitioner's Guide," *Annual Review of Public Health* 37 (2016): 17–32.

7. E. J. Tchetgen Tchetgen, "On Causal Mediation Analysis With a Survival Outcome," *International Journal of Biostatistics* 7, no. 1 (2011): 1–38.

8. Y. Zhao and X. Luo, "Granger Mediation Analysis of Multiple Time Series With an Application to Functional Magnetic Resonance Imaging," *Biometrics* 75, no. 3 (2019): 788–798.

9. M. A. Lindquist, "Functional Causal Mediation Analysis With an Application to Brain Connectivity," *Journal of the American Statistical Association* 107, no. 500 (2012): 1297–1309.

10. S. Zeng, S. Rosenbaum, S. C. Alberts, E. A. Archie, and F. Li, "Causal Mediation Analysis for Sparse and Irregular Longitudinal Data," *Annals of Applied Statistics* 15, no. 2 (2021): 747–767.

11. Y. T. Huang and W. C. Pan, "Hypothesis Test of Mediation Effect in Causal Mediation Model With High-Dimensional Continuous Mediators," *Biometrics* 72, no. 2 (2016): 402–413.

12. O. Y. Chén, C. Crainiceanu, E. L. Ogburn, B. S. Caffo, T. D. Wager, and M. A. Lindquist, "High-Dimensional Multivariate Mediation With Application to Neuroimaging Data," *Biostatistics* 19, no. 2 (2017): 121–136.

13. Y. Song, X. Zhou, M. Zhang, et al., "Bayesian Shrinkage Estimation of High Dimensional Causal Mediation Effects in Omics Studies," *Biometrics* 76, no. 3 (2020): 700–710.

14. Y. Zhao, M. A. Lindquist, and B. S. Caffo, "Sparse Principal Component Based High-Dimensional Mediation Analysis," *Computational Statistics & Data Analysis* 142 (2020): 106835.

15. Y. Zhao and X. Luo, "Pathway Lasso: Pathway Estimation and Selection With High Dimensional Mediators," *Statistics and Its Interface* 15, no. 1 (2022): 39–50.

16. M. T. Aung, Y. Song, K. K. Ferguson, et al., "Application of an Analytical Framework for Multivariate Mediation Analysis of Environmental Data," *Nature Communications* 11, no. 1 (2020): 1–13.

17. J. P. Long, E. Irajizad, J. D. Doecke, and H. M. J. Do KA, "A Framework for Mediation Analysis with Multiple Exposures, Multivariate Mediators, and Non-Linear Response Models," *arXiv preprint arXiv:2011.06061* 2020.

18. R. R. Zhou, L. Wang, and S. D. Zhao, "Estimation and Inference for the Indirect Effect in High-Dimensional Linear Mediation Models," *Biometrika* 107, no. 3 (2020): 573–589.

19. Q. Zhang, "High-Dimensional Mediation Analysis With Applications to Causal Gene Identification," *Statistics in Biosciences* 14 (2021): 1–20.

20. Y. Zhao and L. Li, "Multimodal Data Integration via Mediation Analysis With High-Dimensional Exposures and Mediators," *Human Brain Mapping* 43, no. 8 (2022): 2519–2533.

21. R. M. Baron and D. A. Kenny, "The Moderator–Mediator Variable Distinction in Social Psychological Research: Conceptual, Strategic, and Statistical Considerations," *Journal of Personality and Social Psychology* 51, no. 6 (1986): 1173.

22. C. Nitzl, J. L. Roldan, and G. Cepeda, "Mediation Analysis in Partial Least Squares Path Modeling: Helping Researchers Discuss More Sophisticated Models," *Industrial Management & Data Systems* 116, no. 9 (2016): 1849–1864.

23. G. C. Carrión, C. Nitzl, and J. L. Roldán, "Mediation Analyses in Partial Least Squares Structural Equation Modeling: Guidelines and Empirical Examples," in *Partial Least Squares Path Modeling Basic Concepts, Methodological Issues and Applications* (Cham, Switzerland: Springer, 2017), 173–195.

24. K. Imai and T. Yamamoto, "Identification and Sensitivity Analysis for Multiple Causal Mechanisms: Revisiting Evidence From Framing Experiments," *Political Analysis* 21, no. 2 (2013): 141–171.

25. T. J. VanderWeele, *Explanation in Causal Inference: Methods for Mediation and Interaction* (New York, NY: Oxford University Press, 2015).

26. J. Doshi, G. Erus, Y. Ou, et al., "MUSE: MUlti-Atlas Region Segmentation Utilizing Ensembles of Registration Algorithms and Parameters, and Locally Optimal Atlas Selection," *NeuroImage* 127 (2016): 186–195.

27. M. E. Sobel, "Asymptotic Confidence Intervals for Indirect Effects in Structural Equation Models," *Sociological Methodology* 1982, no. 13 (1982): 290–312.

28. B. Efron, "Better Bootstrap Confidence Intervals," *Journal of the American Statistical Association* 82, no. 397 (1987): 171–185.

29. P. R. Rosenbaum, "Covariance Adjustment in Randomized Experiments and Observational Studies," *Statistical Science* 17, no. 3 (2002): 286–327.

30. R. Tibshirani, "Regression Shrinkage and Selection via the Lasso," *Journal of the Royal Statistical Society: Series B: Methodological* 58, no. 1 (1996): 267–288.

31. H. Zou, T. Hastie, and R. Tibshirani, "Sparse Principal Component Analysis," *Journal of Computational and Graphical Statistics* 15, no. 2 (2006): 265–286.

32. T. Kanekiyo, T. Ban, K. Aritake, et al., "Lipocalin-Type Prostaglandin D Synthase/β-Trace Is a Major Amyloid β-Chaperone in Human Cerebrospinal Fluid," *Proceedings of the National Academy of Sciences* 104, no. 15 (2007): 6412–6417.

33. W. E. Heywood, D. Galimberti, E. Bliss, et al., "Identification of Novel CSF Biomarkers for Neurodegeneration and Their Validation by a High-Throughput Multiplexed Targeted Proteomic Assay," *Molecular Neurodegeneration* 10, no. 1 (2015): 1–16.

34. M. F. Xiao, D. Xu, M. T. Craig, et al., "NPTX2 and Cognitive Dysfunction in Alzheimer's Disease," *eLife* 6 (2017): e23798.

35. L. Dayon, A. N. Galindo, J. Wojcik, et al., "Alzheimer Disease Pathology and the Cerebrospinal Fluid Proteome," *Alzheimer's Research & Therapy* 10, no. 1 (2018): 66.

36. N. D. Beckmann, W. J. Lin, M. Wang, et al., "Multiscale Causal Networks Identify VGF as a Key Regulator of Alzheimer's Disease," *Nature Communications* 11, no. 1 (2020): 1–19.

37. L. W. Bonham, E. G. Geier, N. Z. Steele, et al., "Insulin-Like Growth Factor Binding Protein 2 Is Associated With Biomarkers of Alzheimer's Disease Pathology and Shows Differential Expression in Transgenic Mice," *Frontiers in Neuroscience* 12 (2018): 476.

38. N. Zhao, C. C. Liu, A. J. Van Ingelgom, et al., "APOE ε2 Is Associated With Increased Tau Pathology in Primary Tauopathy," *Nature Communications* 9, no. 1 (2018): 4388.

39. O. Goldhardt, I. Warnhoff, I. Yakushev, et al., "Kallikrein-Related Peptidases 6 and 10 Are Elevated in Cerebrospinal Fluid of Patients

With Alzheimer's Disease and Associated With CSF-TAU and FDG-PET," *Translational Neurodegeneration* 8, no. 1 (2019): 1–13.

40. S. Bhatia, W. S. Kim, C. E. Shepherd, and G. M. Halliday, "Apolipoprotein D Upregulation in Alzheimer's Disease but Not Frontotemporal Dementia," *Journal of Molecular Neuroscience* 67 (2019): 125–132.

41. P. F. Angelo and P. F. Angelo, "Substrate Specificity of Human Kallikrein 6 Salt and Glycosaminoglycan Activation Effects," *Journal of Biological Chemistry* 281, no. 6 (2006): 3116–3126.

42. L. Nadel and O. Hardt, "Update on Memory Systems and Processes," *Neuropsychopharmacology* 36, no. 1 (2011): 251–273.

43. S. Sadigh-Eteghad, A. Majdi, M. Farhoudi, M. Talebi, and J. Mahmoudi, "Different Patterns of Brain Activation in Normal Aging and Alzheimer's Disease From Cognitional Sight: Meta Analysis Using Activation Likelihood Estimation," *Journal of the Neurological Sciences* 343, no. 1-2 (2014): 159–166.

44. T. D. Parker, C. F. Slattery, J. Zhang, et al., "Cortical Microstructure in Young Onset Alzheimer's Disease Using Neurite Orientation Dispersion and Density Imaging," *Human Brain Mapping* 39, no. 7 (2018): 3005–3017.

45. H. I. Jacobs, D. A. Hopkins, H. C. Mayrhofer, et al., "The Cerebellum in Alzheimer's Disease: Evaluating Its Role in Cognitive Decline," *Brain* 141, no. 1 (2018): 37–47.

46. S. A. Schultz, B. A. Gordon, S. Mishra, et al., "Widespread Distribution of Tauopathy in Preclinical Alzheimer's Disease," *Neurobiology of Aging* 72 (2018): 177–185.

47. C. R. Jack, Jr., F. Barkhof, M. A. Bernstein, et al., "Steps to Standardization and Validation of Hippocampal Volumetry as a Biomarker in Clinical Trials and Diagnostic Criterion for Alzheimer's Disease," *Alzheimer's & Dementia* 7, no. 4 (2011): 474–485.

48. S. M. Nestor, R. Rupsingh, M. Borrie, et al., "Ventricular Enlargement as a Possible Measure of Alzheimer's Disease Progression Validated Using the Alzheimer's Disease Neuroimaging Initiative Database," *Brain* 131, no. 9 (2008): 2443–2454.

49. K. Kruthika, H. Maheshappa, and Alzheimer's Disease Neuroimaging Initiative, "Multistage Classifier-Based Approach for Alzheimer's Disease Prediction and Retrieval," *Informatics in Medicine Unlocked* 14 (2019): 34–42.

50. D. O. Hebb, *The Organization of Behavior: A Neuropsychological Theory* (New York: Psychology Press, 2005).

51. A. Charnes, E. L. Frome, and P. L. Yu, "The Equivalence of Generalized Least Squares and Maximum Likelihood Estimates in the Exponential Family," *Journal of the American Statistical Association* 71, no. 353 (1976): 169–171.

52. H. White, "A Heteroskedasticity-Consistent Covariance Matrix Estimator and a Direct Test for Heteroskedasticity," *Econometrica* 48, no. 4 (1980): 817–838.

Supporting Information

Additional supporting information can be found online in the Supporting Information section.